

High-Performance Control of Two Three-Phase Permanent Magnet Synchronous Machines in an Integrated Inverter for Automotive Applications

Lixin Tang
Oak Ridge Associated Universities
Knoxville, TN 37932, USA

Gui-Jia Su
Oak Ridge National Laboratory
Knoxville, TN 37932, USA

Abstract-The closed loop digital signal processor control of an integrated dual inverter, able to independently drive two three-phase permanent magnet motors, is presented. By utilizing the neutral point of the main traction motor, only two inverter legs are needed for the three-phase auxiliary motor. Utilizing this topology, one inverter leg is eliminated and an integrated, reduced component count drive is achieved.

I. INTRODUCTION

The recent success of hybrid electric vehicles (HEVs) is drawing public attention to the power electronic and electric drives used as enabling technologies in these vehicles. Power electronic converters and electric motors are used to partially replace internal combustion engines (ICEs) to achieve higher gas mileage and lower emissions. Ultimately, it is expected that power electronics and electric machines will totally replace ICEs so as to achieve even higher energy efficiency and zero emissions in pure electric vehicles (EVs). In EVs and some HEVs, two major electric drives are necessary: (1) a traction drive to deliver the driving force for the vehicle, and (2) a compressor drive for the air-conditioning (AC) or climate control system. This enables the controller to adjust the cooling or heating without depending on the ICE. Normally the traction drive is rated between 30 and 100 kW [1] and requires fast dynamic response and high efficiency. The compressor drive is rated at a few kilowatts and does not require very high dynamics [2]. Power electronic inverters and control circuits are needed for these two drives. Usually two three-leg inverters are used to achieve independent control. In addition, to achieve high efficiency and power density, permanent magnet (PM) synchronous motors (PMSMs) are chosen for HEV and EV applications.

For automotive applications, reliability and cost are major concerns. Generally, power electronic converter topologies with reduced component counts can reduce the size, weight, and cost of the converter and can also improve reliability [1]. Designs utilizing fewer components with similar or even

reduced functionalities are desired in automotive applications due to these advantages.

Extensive work has been done on a low cost induction motor drive based on a four-switch three-phase inverter (FSTPI) (Fig. 1). A space vector modulation scheme (SVMFSI) without a zero voltage vector was proposed and verified for this topology [3]. It was shown that the output voltage harmonics could be reduced significantly under symmetrical space vector modulation (SVM3). The middle point voltage variation could also be measured and compensated for by an improved SVM scheme in [4] to achieve a more balanced three-phase current at the cost of one more voltage sensor. Using this topology can save two power switches out of six, which is a great achievement. The penalties associated with the topology are a larger alternating current (ac) distortion, which in turn results in a 14% torque ripple at a 4 kHz switching frequency, a doubling of the direct current (dc) bus voltage, and an increased number of capacitors. For automotive applications, a larger current distortion means lower efficiency; and a larger capacitor count means reduced system reliability as well as increased cost, size, and weight, all of which are undesirable. Therefore, the split capacitor bank is not desirable for automobile applications.

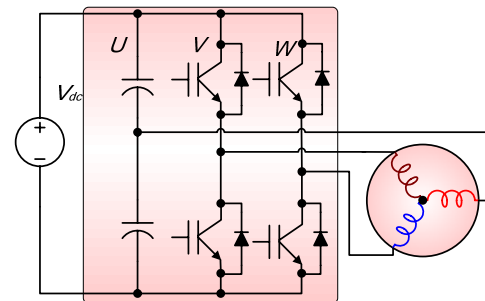


Fig. 1. Split dc bus capacitor FSTPI.

Another method considered to reduce the inverter switch count is to use apportioning technologies as reported in [5]. This scheme does not require extra hardware. It is able to drive one three-phase induction motor and one two-phase induction motor with five inverter legs. Note that the apportioning technology introduces extra distortion to both

* Prepared by Oak Ridge National Laboratory, managed by UT-Battelle, LLC, for the U.S. Dept. of Energy under contract DE-AC05-00OR22725.

The submitted manuscript has been authored by a contractor of the U.S. Government under contract DE-AC05-00OR22725. Accordingly, the U.S. Government retains a nonexclusive, royalty-free license to publish or reproduce the published form of this contribution, or allow others to do so, for U.S. Government purposes.

drives, which may cause degraded performance. For automotive applications, the main traction motor consumes significant amounts of power and requires high efficiency.

To achieve this, an integrated dual inverter without a split capacitor was proposed in [6] and verified with induction motors. The neutral point of the main traction motor was utilized as a return path for the two-phase compressor drive. Experimental results in [6] and [7] show that the zero sequence current from the auxiliary drive did not affect the operation of the main traction motor. Both motors can be controlled independently at different speeds. Closed loop control of two PM motors (i.e., one three-phase PM motor and one two-phase PM motor) was also presented in [8–9]. However, it was found that two-phase PM motors are difficult to find on the market. Hence, control algorithms and topologies for three-phase PM motors are more desirable.

In this paper, the topology used to drive two-three phase PM motors in a closed loop manner is presented, as indicated in Fig. 2. Note that the power ratings of the two motors are sufficiently different so that the current of the auxiliary motor will not cause significant loss in the main motor. The limitation of this scheme is that it is applicable only to Y-connected main traction motors, which is true for the majority of cases in EV/HEV applications.

This paper is organized as follows: Section II proposes and explains the control algorithms for the two three-phase PMSM drives in the integrated inverter; Section III provides the dynamic and steady state modeling results; Section IV shows the hardware setup used in the project and some experimental results; Section V points out the limitations of the proposed scheme; and finally Section VI presents conclusions.

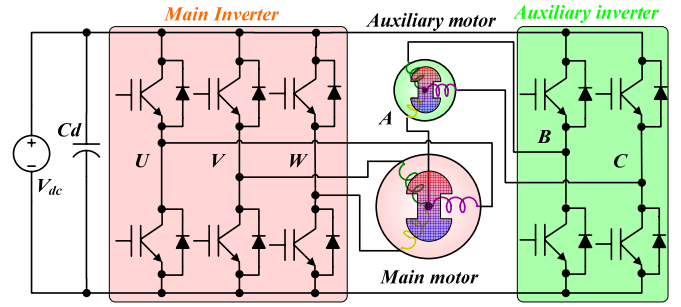


Fig. 2. Integrated inverter for driving two three-phase motors.

II. CONTROL ALGORITHMS FOR TWO THREE PHASE PM MOTORS

Rotor flux oriented control (RFOC) is widely used in high performance PM motor drives. To control two three-phase PM motors with this dual inverter, some modifications are necessary. A block diagram of the RFOC algorithm is shown in Fig. 3. The neutral point of the main PM motor is used as a return path for the auxiliary motor, and thus a zero sequence current will be flowing to the neutral point and appears in the measured traction motor currents by the current sensors. Therefore, the zero sequence current has to be removed before the Park transform, as indicated in Fig. 3. Although using one current sensor in each phase of the main PM motor gives the zero sequence current, this method is rarely used in industrial applications because of the higher cost. Note that the zero sequence current contributes neither to the torque nor the flux in the main PM motor. A detailed explanation can be seen in [6].

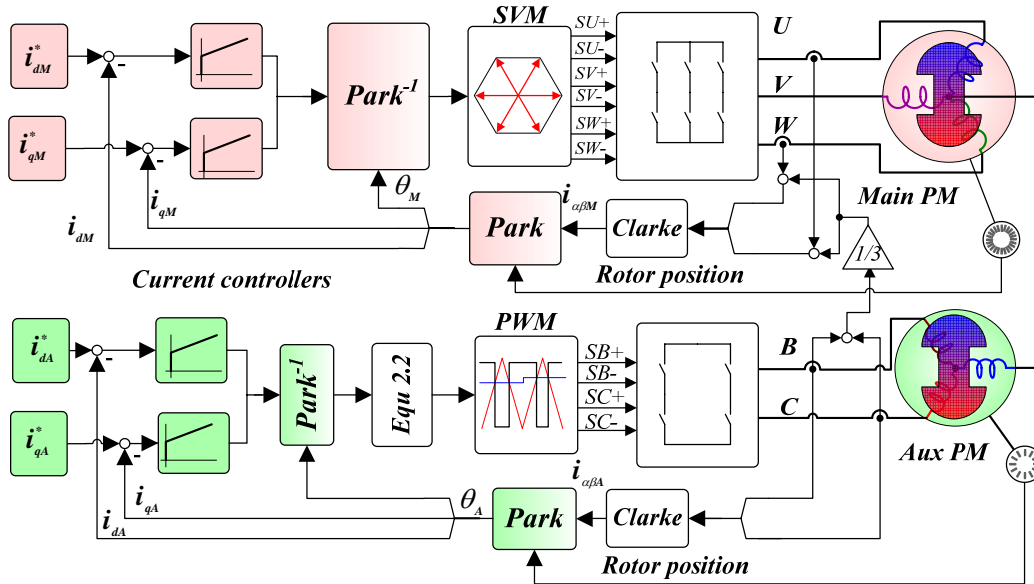


Fig. 3. Control block diagram of the proposed integrated inverter.

For the auxiliary motor shown in Fig. 3, it is obvious that the phase-A voltage is no longer controllable. It is equal to the neutral point voltage of the main three phase PM motor and will fluctuate about one half of the dc bus voltage depending on the switching states of the main inverter. Only phase B and C voltages can be controlled. A control law must be developed to regulate the two currents via the phase B and C voltage, under this condition.

For a voltage source inverter, it is always preferred to know the reference voltages such that they can be used to generate the desired switching pulses precisely. For a normal three-phase motor driven by a three-phase inverter, the three reference voltages can be obtained by solving Eq. (1) with known values for u_α , u_β , and u_0 . In the case of the auxiliary motor, only phase B and C reference voltages are needed. Assuming phase A voltage, u_a , is known, phase B and C voltages can be found, as shown in Eq. (2). This is the basis for the control algorithm to be used for the auxiliary motor vector control. The appearance of u_a in Eq. (2) does not mean that phase A voltage needs to be measured by a voltage sensor. In the closed loop control, the phase B and C currents will be regulated by a proportional integral type controller and any variation of the voltages (dc bus voltage and phase A voltage) will be corrected. Therefore, accurate phase A voltage is not necessary for this scheme.

$$\begin{bmatrix} u_\alpha \\ u_\beta \\ u_0 \end{bmatrix} = \frac{2}{3} \begin{bmatrix} 1 & -\frac{1}{2} & -\frac{1}{2} \\ 0 & \frac{\sqrt{3}}{2} & -\frac{\sqrt{3}}{2} \\ \frac{1}{2} & \frac{1}{2} & \frac{1}{2} \end{bmatrix} \begin{bmatrix} u_a \\ u_b \\ u_c \end{bmatrix}. \quad (1)$$

$$\begin{cases} u_b = \frac{1}{2}(2u_a - 3u_\alpha + \sqrt{3}u_\beta) \\ u_c = \frac{1}{2}(2u_a - 3u_\alpha - \sqrt{3}u_\beta) \end{cases}. \quad (2)$$

III. MODELING RESULTS

To verify the proposed closed loop algorithm, computer modeling was carried out with Psim® software. The Psim model consists of two PM motors; one as the main motor and the other as the auxiliary motor. The two controllers illustrated in Fig. 3. were used to control the two PM motors. The parameters of the two PM motors are shown in Appendix 1. The zero sequence equivalent circuit of the main motor was used in the modeling work. The current from the auxiliary motor to the main motor was a zero sequence component; it

generates some copper and iron losses but will not generate any net torque in the main motor. However, since the amplitude of the zero sequence current is small, the extra losses are negligible compared to the other losses in the main motor. Details of the extra loss calculation will be shown in Section V.

The steady state currents of the two three-phase PM motors are shown in Fig. 4. The waveforms in the top plot are the three phase currents in the auxiliary motor and the bottom plot shows the three phase currents in the main motor. It is seen that the three phase currents in the auxiliary motor are smooth sinusoids. However, in the main motor, although the current waveforms are close to sinusoidal, there are small fluctuations in the currents, caused by the zero sequence current. Note that the amplitude of the zero sequence component is quite small compared with the fundamental component of the main motor current.

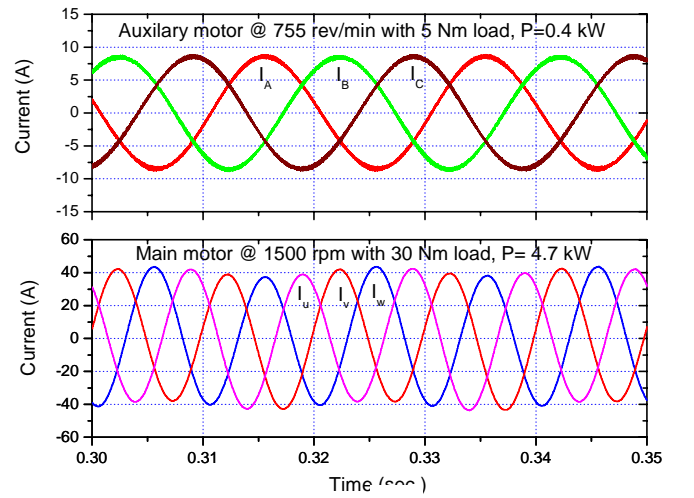


Fig. 4. Currents of the main and auxiliary motors (modeling results).

The d - q axis currents and q axis current reference of the two motors are shown in Fig. 5; the d axis reference current is zero for both motors. The top and bottom plots show the d and q axis currents of the auxiliary and main motors, respectively. The actual q axis current reaches the reference value quickly and follows the reference closely in both cases. The reference and actual currents almost overlap all the time; the d axis currents stay at zero. The d axis currents are set to zero because both the motors are surface mounted PM motors, and field weakening cannot be implemented with a meaningful speed range in this case.

From the modeling results, it is seen that the proposed algorithm is able to control the currents in two three phase PM motors, both in steady state and dynamic states.

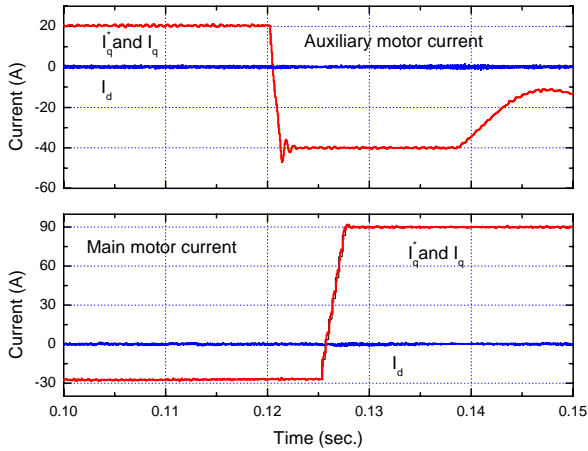


Fig. 5. Currents of the main and auxiliary motors in their own d - q frames (modeling results).

Note that in both cases the actual voltage of the main motor neutral point is not used. The fixed value of half of the dc bus voltage is used instead in the controller. It confirms that the regulators can overcome the error between the assumed voltage and actual voltage at the neutral point of the main motor.

IV. EXPERIMENTAL RESULTS

An integrated dual inverter was constructed for experimental verification. It has two kinds of insulated gate bipolar transistor (IGBT) modules; one with a large power rating for the three-phase main drive and the other with a smaller rating for the two-phase inverter auxiliary drive. All power modules were mounted on a liquid cooled cold plate. The dc bus voltage was set to 325 V, and four Hall effect current sensors were employed to detect the currents. Film capacitors rather than electrolytic capacitors were used for dc bus filtering, which was desirable due to their superior reliability. The switching frequency was set to 15 kHz for both inverters.

The system diagram of the experimental setup is shown in Fig. 6. The main traction motor was an 8.2 kW PMSM, the auxiliary motor was a three-phase 5.5 kW PMSM, manufactured by Allen-Bradley. An eddy current dynamometer was used to load the auxiliary motor. The parameters of the two PM motors are listed in Appendix 1.

A digital signal processor (DSP) card fabricated at Oak Ridge National Laboratory (ORNL) was employed to implement the real time control algorithm. The controller board was based on a TMS320F2812 DSP chip from Texas Instruments running at a clock frequency of 150 MHz (6.67 ns cycle time). The DSP's two event managers were used to generate the pulse width modulation (PWM) pulses for the

two PM motors. Two incremental encoders were employed to obtain the rotor positions of the two motors. The starting schemes explained in [8] were used.

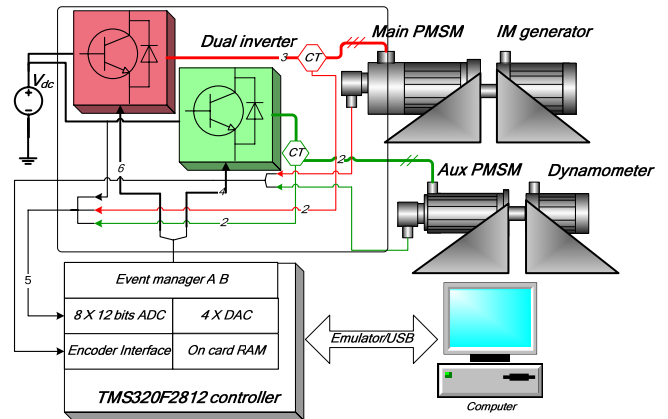


Fig. 6. Experimental setup for the dual inverter project.

Figure 7 shows the current waveforms of the two PM motors with the main motor stopped and the auxiliary motor running at 750 rev/min with a 12 N·m load. The top three traces, ch1, ch2, and ch3 are respectively the phases U, V, and W currents of the main traction motor. The bottom three traces are currents of phases A, B, and C of the auxiliary motor, respectively. The scales are 50 A/div for the currents with a time scale of 10 ms/div. It is seen that the currents in the auxiliary motor are sinusoidal and the currents in the main motor are almost identical; each equals one third of the phase A current in the auxiliary motor. Note that even if the main motor is not running, it is still required to switch the main inverter at 50% duty so that the current can flow back to the dc bus.

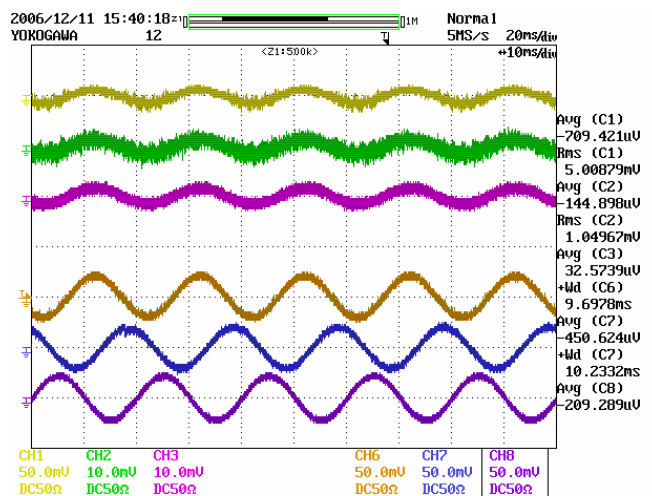


Fig. 3. Currents of the main and auxiliary motors (experimental results). CH1: i_u , CH2: i_v , CH3: i_w , 50A/div; CH6: i_a , CH7: i_b , CH8: i_c , 50A/div; main motor: 0 rpm, 0 N·m; auxiliary motor: 750 rpm, 12 N·m

Figures 8 and 9 show modeling and experimental results at identical operating conditions. The main motor is running at

200 rev/min without a load, and the auxiliary motor is running at 500 rev/min with the rated load torque. Sinusoidal currents are observed in the auxiliary motor, both in the modeling and experimental results. The main motor carries a balanced three-phase current and, superimposed on each phase, one third of the phase A current of the auxiliary motor, as indicated in Figs. 8 and 9. It is seen that there is more ripple components in the main motor currents, especially in the experimental results. This is possibly because a smaller scale is used for the current probes when measuring the main motor current, and therefore the measured traces are more susceptible to switching noises.

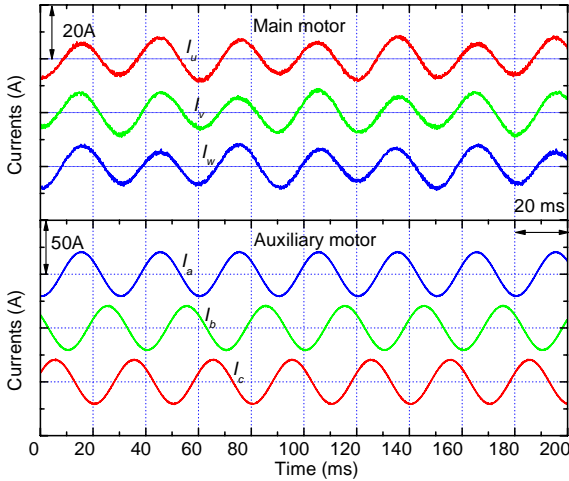


Fig. 8. Currents of the main and auxiliary motors (modeling results). The main motor runs at 200 rpm with 0 N·m load; the auxiliary motor runs at 500 rpm with 12 N·m load.

running at 750 rev/min with rated load in both figures. Almost matching results are seen again, with clean sinusoidal current waveforms in the auxiliary motor. Again there are two major frequency components in the main motor current; one is for driving the main motor, and the other is one third of the phase A current of the auxiliary motor.

From these results, it is confirmed that both motors can be regulated independently in the integrated, reduced component count inverter.

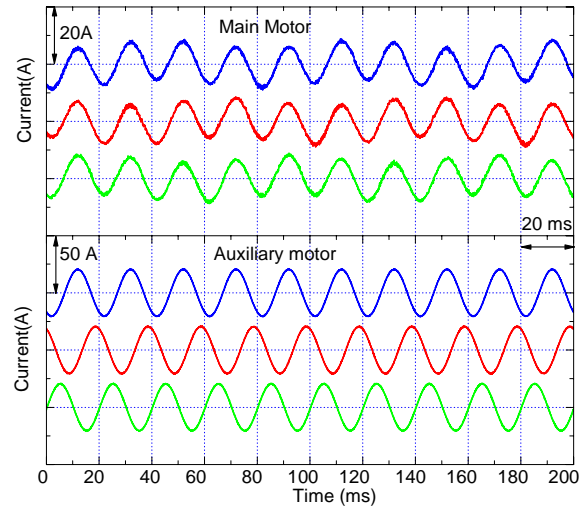


Fig. 10. Currents of the main and auxiliary motors (modeling results). The main motor runs at 200 rpm with 0 N·m load; the auxiliary motor runs at 750 rpm with 12 N·m load.

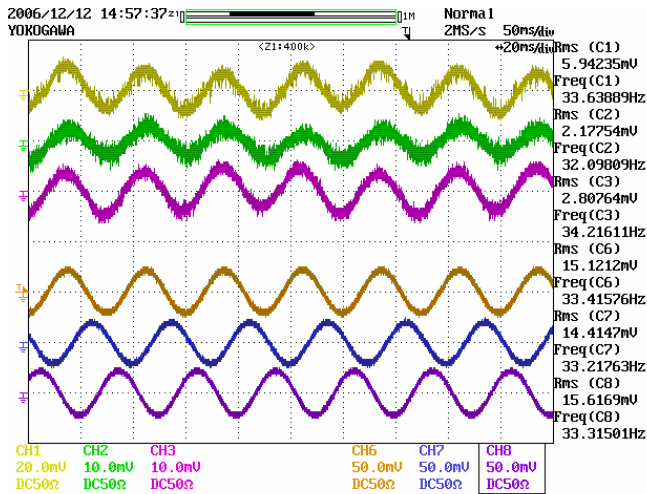


Fig. 9. Currents of the main and auxiliary motors (experimental results). CH1: i_u , CH2: i_v , CH3: i_w , 20A/div; CH6: i_a , CH7: i_b , CH8: i_c , 50A/div; main motor: 200 rpm, 0 N·m; auxiliary motor: 500 rpm, 12 N·m.

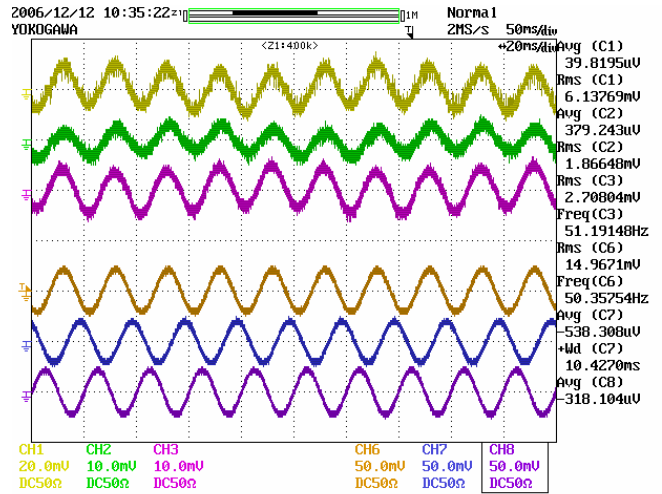


Fig. 11. Currents of the main and auxiliary motors (experimental results). CH1: i_u , CH2: i_v , CH3: i_w , 20A/div; CH6: i_a , CH7: i_b , CH8: i_c , 50A/div; main motor: 200 rpm with 0 N·m load; the auxiliary motor: 750 rpm with 12 N·m load.

Figures 10 and Fig. 11 show modeling and experimental results of the two motors, respectively with the main motor running at 200 rev/min with no load and the auxiliary motor

V. LIMITATIONS OF THIS SCHEME AND DISCUSSIONS

So far, the modeling and experimental results show that this topology is able to control two three-phase PM motors independently, resulting in the elimination of one inverter leg. However, the tradeoffs of this circuit should also be addressed, so that a complete view of this topology can be obtained.

A. EXTRA COPPER LOSS IN THE MAIN MOTOR

Because the auxiliary motor current flows in the main motor, it results in extra losses in the main motor and inverter. The extra loss in the main motor can be calculated by

$$P_e = 3 \times \frac{I}{9} I_{Arms}^2 R_M = \frac{I}{3} I_{Arms}^2 R_M, \quad (3)$$

where R_M is the phase resistance of the main motor and I_{Arms} the rated current of the auxiliary motor. The extra loss can be expressed as a percentage of the copper loss due to the main motor's own fundamental current by

$$\Delta p = 100 \times \left(\frac{I_{Arms}^2}{3 \times I_{Mrms}^2} \right), \quad (4)$$

where I_{Mrms} is the rated current of the main motor. The relationship between the current ratio (defined as I_{Main}/I_{Aux}) and the extra loss (%) in the main motor is plotted in Fig. 12. The extra loss is as low as about 4%, when the current ratio is 3. As the current ratio increases, the extra loss drops significantly, as shown in the figure. The result shows the extra copper loss in the main motor is negligible (less than 1% increase) when the current ratio is larger than 6.

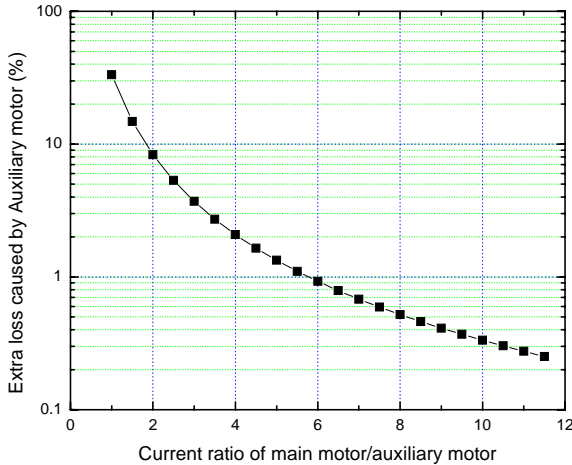


Fig. 12. Relationship between the current ratio and extra copper loss in the main motor.

B. MAXIMUM OUTPUT VOLTAGE OF THE AUXILIARY INVERTER

By utilizing the proposed topology, an inverter leg can be eliminated in the auxiliary motor drive, while sinusoidal voltage operation and closed loop control can still be achieved. However, note that due to phase A voltage of the auxiliary motor is almost fixed to half of the dc bus voltage, and the amplitude of the voltage vector applicable to the auxiliary motor is only half of that generated by a three leg inverter counterpart, as indicated in Fig. 13. Therefore, the number of stator windings of the auxiliary motor needs to be chosen properly to generate the same power.

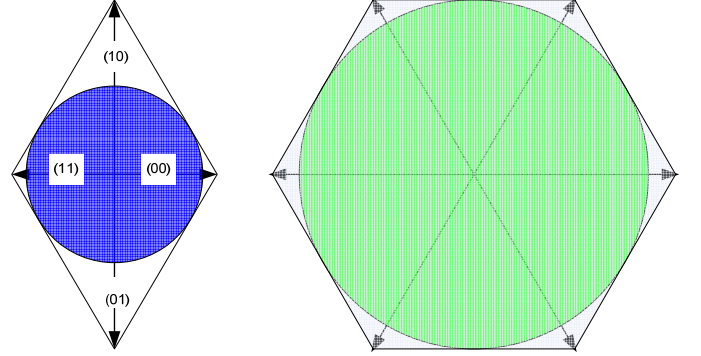


Fig. 13. Amplitude of the maximum output voltage vector. The maximum output voltage circle of the proposed inverter (left), the maximum output voltage circle generated by a three phase inverter with three inverter legs (right).

VI. CONCLUSIONS

In this paper, the control algorithm for driving two three-phase PM motors in the reduced component count dual integrated inverter is presented and tested. It is an extension of closed loop control of the schemes proposed for induction machines in [6] and PM machines in [8,9]. Modeling and experimental results at various loads and speeds of two three phase motors are shown to confirm that the two motors can be controlled independently under the proposed scheme. A low cost, integrated drive for automotive applications has been achieved.

Although the control scheme was proposed and verified with PM motors, it should be noted that it is also applicable to other types of ac motors. The control algorithm proposed in Section II can also be used for the split dc bus capacitor FSTPI for closed loop control.

This paper also addressed two tradeoffs of the proposed integrated drives: (1) the reduction in the maximum output voltage of the auxiliary inverter needs to be taken into account in selection of the auxiliary motor, and (2) the extra copper loss in the main motor caused by the auxiliary motor current is negligible when the current ratio is larger than 6, which is quite easy to satisfy in many EV/HEV drive systems.

APPENDIX 1. Parameters of the two PM motors used in this project

Name of the parameters	Main Motor	Auxiliary Motor
Rated output power (W)	8200	5500
Rated speed (rev/min)	2000	4000
Rated voltage (V, rms)	200	230
Rated current (A, rms)	52.7	18.9
Back EMF constant (V/1000 rpm, L-L voltage, 0 to peak)	88.1	71.25
Poles	8	8
Rated torque (Nm)	39.4	13.1
Stator resistance (Ω)	0.03	0.2
Stator inductance (mH)	0.99	1.5
Inertia (kg.m ²)	0.019	0.00147

REFERENCES

- [1] M. Kamiya, "Development of Traction Drive Motors for the Toyota Hybrid System," pp. 1474–1481 in *2005 International Power Electronics Conference (IPEC 2005)*, 2005.
- [2] M. Naidu, M. T. W. Nehl, S. Gopalakrishnan, and L. Wurth, "Keeping Cool While Saving Space and Money: A Semi-Integrated, Sensor-Less PM Brushless Drive for a 42-V Automotive HVAC Compressor," pp. 20–28 in *IEEE Industry Applications Magazine* **11**(4), July–August 2005.
- [3] F. Blaabjerg, S. Freyswson, H. Hansen, and S. Hansen, "A New Optimized Space-Vector Modulation Strategy for a Component-Minimized Voltage Source Inverter," pp. 704–714 in *IEEE Trans. Power Electronics* **12**(4), July 1997.
- [4] F. Blaabjerg, D. O. Neacsu, and J. K. Pedersen, "Adaptive SVM to Compensate DC-Link Voltage Ripple for Four-Switch Three-Phase Voltage-Source Inverters," pp. 743–752 in *IEEE Transactions on Power Electronics*, **14**(4), July 1999.
- [5] C. B. Jacobina, O. I. Da Silva, E. C. dos Santos, Jr., and A. M. N. Lima, "Dual AC Drives with Five-Leg Converter," pp.1800–1806 in *Power Electronics Specialists Conference, 2005 (PESC'05)*, August 2005.
- [6] G.-J. Su and J. S. Hsu, "A Five-Leg Inverter for Driving a Traction Motor and a Compressor Motor," pp. 117–123 in *8th IEEE Workshop on Power Electronics in Transportation (WPET 2004)*, Novi, Michigan, October 21–22, 2004.
- [7] G.-J. Su and J. S. Hsu, "An Integrated Traction and Compressor Drive System for EV/HEV Applications," pp.719–725 in *Applied Power Electronics Conference and Exposition 2005 (APEC 2005)*, 20th Annual IEEE, **2**, March 6–10, 2005.
- [8] L. Tang, G.-J. Su, and X. Huang, "Experimental High Performance Control of Two Permanent Magnet Synchronous Motors in an Integrated Inverter for Automotive Applications," pp. 186–192 in *Proceedings of the Tenth IEEE COMPEL Workshop, Albany, NY, 2006*, ISBN:0-7803-9725-8, IEEE catalog number: 06TH8893C.
- [9] G.-J. Su, L. Tang, and X. Huang, "Control of Two Permanent Magnet Machines Using Five-Leg Inverter for Automotive Applications" in *Proceedings of the 41st IEEE Industry Application Society Annual Meeting 2006*, Tampa, Florida, USA, ISBN:1-4244-0365-0, IEEE catalog number: 06CH37801C.